Hindawi
Geofluids
Volume 2024, Article ID 1592800, 13 pages
https://doi.org/10.1155/2024/1592800

WILEY | Hindawi

Research Article

Logging Response Mechanism and Content Evaluation of Laumontite-Bearing Glutenite Reservoir: A Case Study of Lower Urho Formation of Permian of the Junggar Basin

Jia Jun [1] **Xue Kunlin,** [2] **Ni Liping,** [3] **Luo Yang,** [4] **and Liu Yuchao** [4]

[1] *College of Resource & Environmental Engineering, Mianyang Normal University, Mianyang 621000, Sichuan, China*
[2] *Geological Research Institute of Baikouquan Oil Production Division of PetroChina Xinjiang Oilfield, Karamay 834000, Xinjiang, China*
[3] *Xinjiang Branch of CNPC Logging Co., Ltd., Karamay 834000, Xinjiang, China*
[4] *College of Energy, Chengdu University of Technology, Chengdu 610059, Sichuan, China*

Correspondence should be addressed to Jia Jun; jj_reec@mtc.edu.cn

Received 9 October 2023; Revised 28 January 2024; Accepted 5 February 2024; Published 6 March 2024

Academic Editor: Shuyang Liu

The Urho Formation in the Lower Permian System at the Junggar Basin in China commonly develops zeolite cements. The presence of zeolite minerals in various states of occurrence and uneven distribution in glutenite reservoirs makes it indeterminate to interpret the well logging response characteristics such as acoustic, resistivity, radioactivity, and nuclear magnetic resonance (NMR). This poses significant challenges for the evaluation of well loggings in glutenite reservoirs containing laumontite and the determination of oil and gas reserves. In this study, through petrophysics experiments such as whole-rock X-ray diffraction, conventional petrophysical properties, mercury injection, and electron microprobe analysis, the characteristics of glutenite reservoirs containing laumontite and the well logging response mechanisms were analyzed from the perspectives of mineral composition of rocks, geochemical characteristics, and principle of loggings. A multimineral optimization method was used to calculate the laumontite content. The results indicate that in the study area, the cementation of zeolite minerals dominated by laumontite suppresses the pore development in the reservoir, which is a crucial factor in the formation of complex pore structures and low-porosity low-permeability reservoirs. Since laumontite exhibits a water-bearing framework structure with numerous micropores and crystal water, the laumontite-bearing glutenite reservoirs are characterized by low natural gamma radiation, low density, high neutron porosity, and high electrical resistivity. The acoustic interval transit time shows no significant differences, while the NMR T_2 spectrum exhibits a short relaxation time.

1. Introduction

The tight glutenite reservoirs of oil and gas are widely distributed globally. Since the discovery of the world's first sandstone oil field, the Tupungato Oil Field in the Cuyo Basin of Argentina in 1934, similar sandstone oil reserves of varying sizes have been successively found in the Pembina Oil Field in Western Canada [1], the Sergipe-Alagoas Basin in Brazil, the North Sea Basin in the United Kingdom [2, 3], the Bohai Bay Basin in Eastern China [4], the Songliao Basin in Northeastern China [5], and the Junggar Basin in Northwestern China [6]. These discoveries have a history of exploration and development spanning nearly a century.

The Junggar Basin, located in the northwestern part of China, is the second-largest basin in China and also one of its important oil and gas resource bases [7]. Since exploration efforts began in the 1930s, the basin has yielded various types of oil and gas resources, including shale oil, tight sandstone oil (gas), coalbed methane, and biogas [8, 9]. Particularly since 2010, there have been continuous new discoveries in the Lower Permian tight glutenite reservoirs such as the Urho Formation and Baikouquan Formation at the

Mahu Lake Depression in the northwest margin of the basin, making them the key areas for oil and gas exploration.

Tight glutenite reservoirs are formed in nearby provenance depositional systems such as alluvial fans, proluvial fans, and fan deltas caused by rapid, unstable, and strong water flows [10]. These reservoirs have a complex lithology, a wide range of size fractions in the skeleton grains [11], developing nanoscale pore throats, complex pore structures [12], and generally poor physical properties [13]. Additionally, due to various diagenesis in the later stages, the tight glutenite reservoirs exhibit the characteristics of low rock maturity, significant physical property variations, strong heterogeneity, and rapid lateral changes [13], resulting in difficulties in the logging evaluation of glutenite reservoirs. With the geological context mentioned above, the Urho Formation in the Lower Permian System at the Junggar Basin commonly develops zeolite group minerals in its tight glutenite reservoirs. The occurrence of these minerals is complex and unevenly distributed, further complicating the reservoir characteristics and increasing the difficulty of logging evaluation.

The study of zeolite group minerals began in the 1960s when Hay [14] initially identified the global distribution of zeolite group minerals. Subsequently, researchers such as Iijima [15], Boles [16], and Utada [17] conducted analyses of the formation environments of zeolites in different regions. Surdam [18], Levy [19], Chipera et al. [20], Zhu et al. [21], and others further investigated the controlling factors of zeolite minerals formation, including formation water properties, mineral composition, temperature, and pressure. Moncure [22] investigated the vertical zonation of zeolite minerals and its diagenetic model. Iijima [23] revealed the controlling role of zeolites in the development of porosity in reservoirs within oil fields. Fercia [24] determined the different cation exchange capacities of zeolite minerals through experiments. Li et al. [25], Zhu et al. [26], Xi et al. [27], and others analyzed the evolutionary sequences of zeolites and explored the relationship between zeolite minerals and hydrocarbon accumulation. Previous research has mainly focused on the issues such as the classification of zeolite minerals, diagenetic processes, and controlling factors of their distributions. However, there are few reports on the characteristics of glutenite reservoirs containing zeolite minerals and the response mechanism of geophysical loggings. It has been found that the logging response characteristics of zeolite-bearing reservoirs in the Lower Permian Urho Formation at the Junggar Basin are highly similar with the oil reservoir characteristics, making fluid identification challenging. The lack of systematic research on the unique characteristics and logging response mechanisms of these special glutenite reservoirs has posed significant challenges for logging evaluation, layer selection test, and reserve estimation in these glutenite reservoirs with laumontites. To address the aforementioned issues, this study conducted research on the characteristics of glutenite reservoirs containing laumontites based on a systematic petrophysics experimental approach. From multiple perspectives including mineral composition of rocks, geochemical properties, and logging principles, the logging response characteristics and formation mechanism of glutenite reservoirs containing laumontites were analyzed and the laumontite content was quantitatively calculated based on multimineral model optimization method. This research provides useful references for effectively identifying laumontite-bearing glutenite reservoirs, improving logging evaluation accuracy, and increasing reserve scale.

2. Geological Setting

The YB4 well area is located at the Luliang Uplift and Yingxi Depression in the western part of the Junggar Basin, China, adjacent to the Mahu Lake Depression. It has undergone multiphase reconstructions by tectonic movements, including the Hercynian, Indosinian, Yanshanian, and Himalayan [28]. The top boundary of the Lower Urho Formation in this area is a southwest-tilted monocline with localized development of nose structures, and it falls under the category of fault-lithology traps (Figure 1).

The strata development in the Permian System of the Junggar Basin can be categorized as the Xiazijie Formation, Lower Urho Formation, Fengcheng Formation, and Jiamuhe Formation (Figure 1). Based on lithological and electrical characteristics, the Lower Urho Formation can be divided into four intervals, referred to as the first interval of P_2w_1 to the fourth interval of P_2w_4 from bottom to top. The Urho P_2w_4 interval is primarily characterized by denudation, with the upper part consisting of deep gray mudstone and sandy mudstone formed by unconformity weathering crust and the middle-lower part composed of gray and grayish brown glutenite. The lithology of the P_2w_3 interval is mainly light brown and gray glutenite and the interbed of inequigranular sandstone with siltstone and mudstone [29].

3. Samples and Methods

In this study, plunger rock samples were collected from the Lower Permian Urho Formation at the Junggar Basin. A series of comprehensive rock petrophysics experiments, including whole-rock X-ray diffraction (XRD), conventional physical measurements, mercury injection (MI), casting thin sections (CTS), and electron microprobe analysis (EM) were then conducted. Based on the core location, high-resolution logging data were collected at the depths corresponding to the rock samples. Due to the strong stress sensitivity and susceptibility to fracturing of the glutenites containing laumontite, they were obtained using the diamond wire cutting method and prepared into 250 mm × 500 mm plunger rock samples.

XRD experiments were conducted following the Chinese petroleum industry standard (SY/T 5163-2010) using the X'Pert MPD PRO diffractometer to obtain mineral composition information [30, 31].

Petrophysical property experiments were conducted according to the Chinese petroleum industry standard (SY/T 5336-1996) using the CMS-400 automatic porosity and permeability meter to obtain the conventional petrophysical parameters such as porosity and permeability [32]. The CMS-400 has a porosity measurement range of 0.01-40%, a

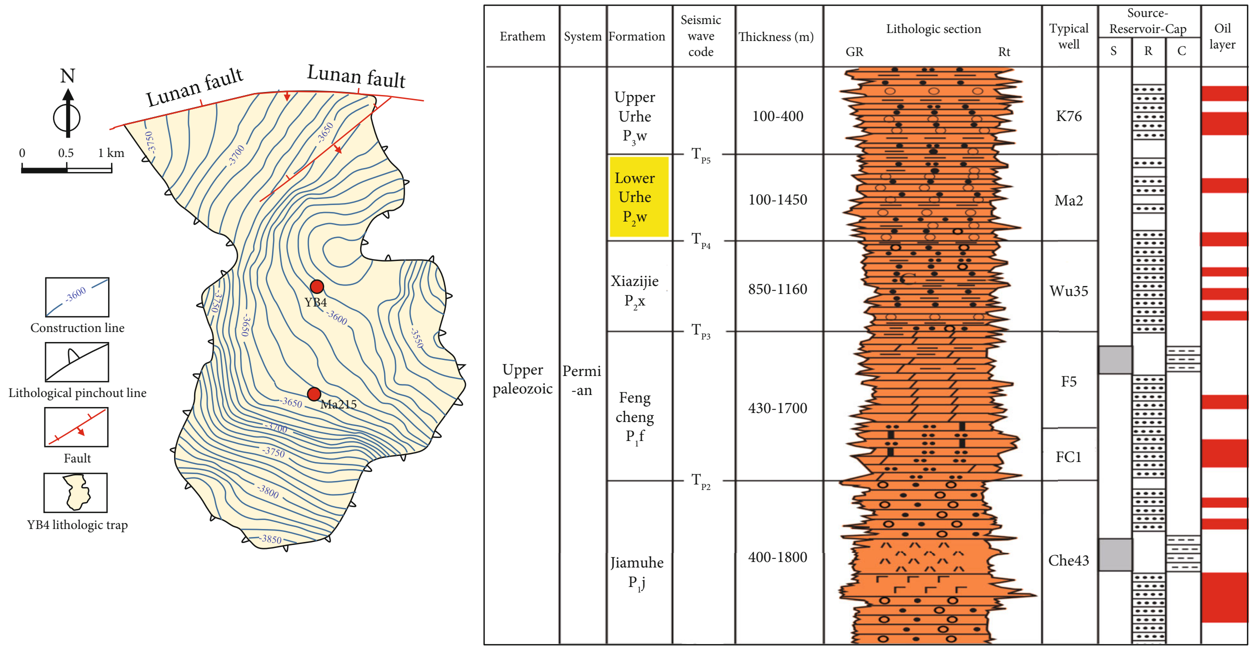

FIGURE 1: Structure and stratigraphic profile of the top boundary of the Permian Lower Urho Formation in well YB4.

permeability measurement range of 0.00005 mD-5 D, and a confining pressure range of 3.5-67.5 MPa.

MI experiments were carried out following the Chinese national standard (GB/T 21650.1-2008) using the American AutoPore 9505 mercury porosimeter (with the maximum mercury injection pressure of up to 413.7 MPa, corresponding to the minimum pore-throat radius of approximately 1.8 nm) to obtain pore-throat distribution characteristics [33–35].

EM experiments were conducted following the Chinese national standard (GB/T 15074-2008) using the EPMA-1720 H Series electron probe microanalyzer to determine the elemental composition of rock minerals [36]. The analysis accuracy for major elements (with concentrations >5%) was ≤1% and was 5% for minor elements (with concentrations <1%).

4. Results

4.1. Petrology Characteristics. From the thin section identification and XRD experimental analysis results, it was found that the gray and brownish gray glutenite dominates the laumontite-bearing glutenite reservoir in the Lower Urho Formation of the YB4 well area (Figure 2). Small sandy glutenite ranks the second, which shows gravel diameters ranging between 2 and 40 mm, and commonly displays subrounded shapes with poor sorting. The dominant mineral components include zeolite, quartz, feldspar, and clay minerals. Among the zeolite group minerals, laumontite is the most abundant, accounting for approximately 33% of the total mineral content, followed by heulandite at about 7.5%. Quartz comprises approximately 27.5% of the mineral content, while feldspar averages around 17.8%. The average clay mineral content is about 12%, predominantly composed of irregular illite/smectite mixed layers, accounting for an average of 47.21% (Table 1).

4.2. Reservoir Physical Property. The results of conventional petrophysical analysis indicated that the Lower Urho Formation belongs to low-porosity and extremely low-permeability reservoirs. In the reservoirs of the Urho P_2w_4 interval where zeolite minerals are developed, the porosity ranges from 2.7% to 19.1%, with an average of 8.5%; the permeability varies from 0.012 mD to 8.06 mD, with an average of 0.051 mD. In the reservoirs of the Urho P_2w_2 interval where zeolite minerals are less developed, the porosity ranges from 7.5% to 19.1%, with an average of 11.38%, and the permeability varies from 0.036 mD to 8.11 mD, with an average of 1.3 mD (Figure 3).

4.3. Characteristics of Reservoir Pore Structure. According to the casting thin section analysis results, the predominant pore types in the reservoirs of the Lower Urho Formation are secondary pores, which include residual intergranular pores, laumontite dissolved pores, and rock waste intragranular dissolved pores. In addition to that, there are also microfractures and shrinkage holes. Zeolite-filled cementation is one of the main types of cementations, and the commonly used zeolite cements include laumontite, heulandite, and analcime. Zeolite cementation can inhibit the development of pores and throats, negatively impacting the reservoir's storage capacity. Mercury injection data revealed that the capillary pressure curves for the reservoirs in the Lower Urho Formation exhibit a moderate skewness. The displacement pressures are relatively high, and the pore sorting is moderate. The maximum pore-throat radius ranges from 0.65 μm to 4.99 μm, with an average of 2.55 μm. The displacement pressure ranges from 0.17 MPa to 0.71 MPa, with an average of 0.44 MPa. The saturation median pressure falls

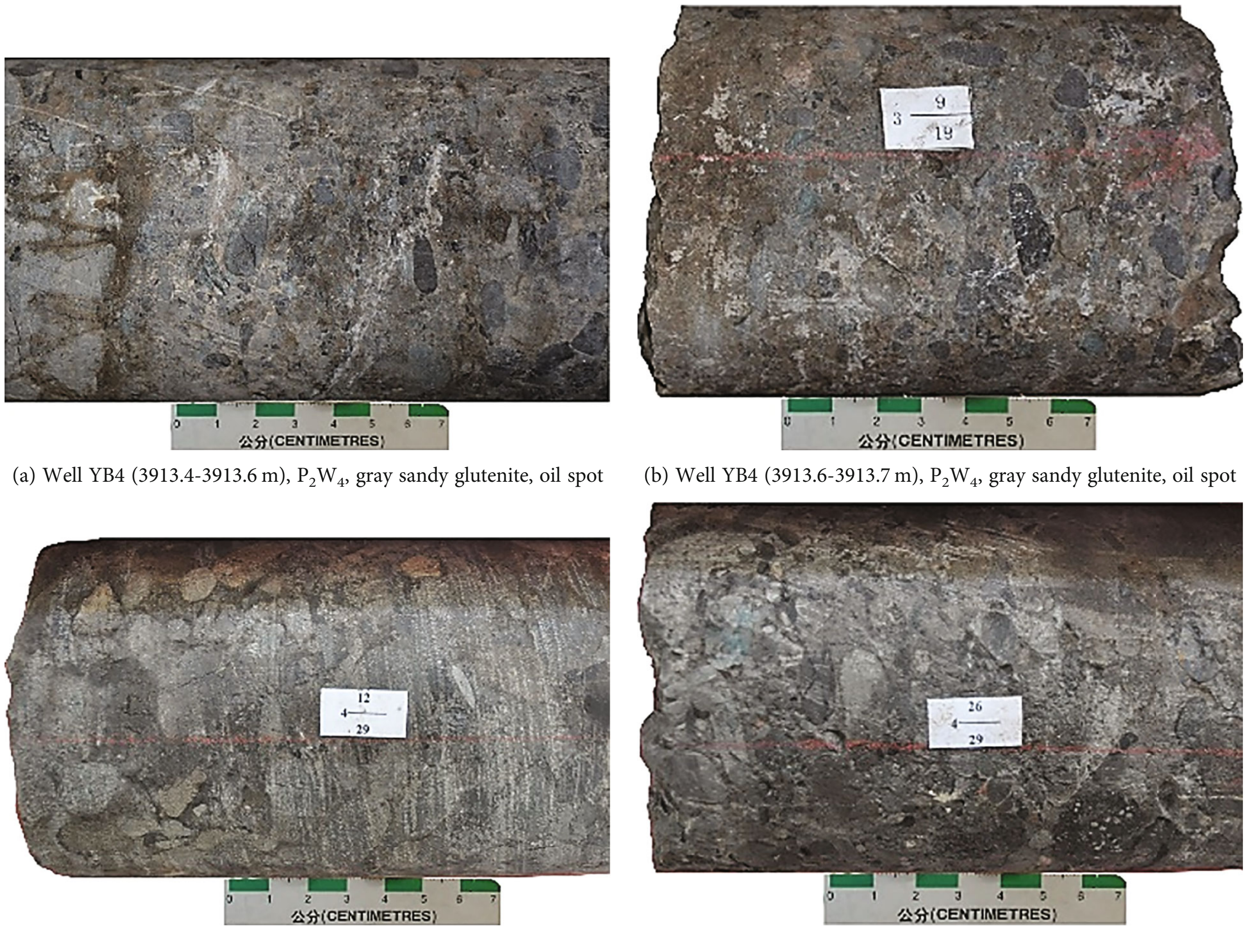

(a) Well YB4 (3913.4-3913.6 m), P_2W_4, gray sandy glutenite, oil spot

(b) Well YB4 (3913.6-3913.7 m), P_2W_4, gray sandy glutenite, oil spot

(c) Well Ma218 (3940.6-3940.74 m), P_2W_4, gray fine to medium glutenite, oil spot

(d) Well Ma218 (3942.9-3943.1 m), P_2W_4, gray fine to medium glutenite, oil spot

Figure 2: Core photos of the Lower Urho Formation of the Permian Lower Urho Formation in well YB4.

Table 1: XRD experimental analysis results.

Whole-rock mineral analysis		Clay mineral analysis	
Mineral types	Mean value (%)	Clay mineral types	Mean value (%)
Laumontite	32.57	Mixed layer of illite and montmorillonite	47.21
Quartz	27.5		
Plagioclase	13.35	Chlorite	32.69
Clay	12	Mixed layer of chlorite and montmorillonite	8.76
Heulandite	7.5		
Potassium feldspar	4.45	Illite	6.56
Calcite	2.48	Kaolinite	4.78
Dolomite	0.15		

between 7.69 MPa and 16.53 MPa, with an average of 10.73 MPa. The saturation median radius ranges from 0.04 μm to 0.1 μm, with an average of 0.07 μm. The mercury withdrawal efficiency varies between 22.49% and 33.75%, with an average of 28.91% (Figure 4).

4.4. Geochemical Properties of Zeolite. Zeolite group minerals are a general term for a group of porous aluminosilicate minerals with a water-bearing framework structure. Currently, over 40 natural zeolites have been identified, with common types including sodium zeolite, calcium zeolite, analcime, laumontite, erionite, and clinoptilolite [37]. According to the X-ray diffraction and electron probe analysis results and their relative abundance, the Lower Urho Formation reservoirs in the study area primarily develops laumontite ($CaAl_2Si_2O_{12}4H_2{\bullet}O$), with less amount of

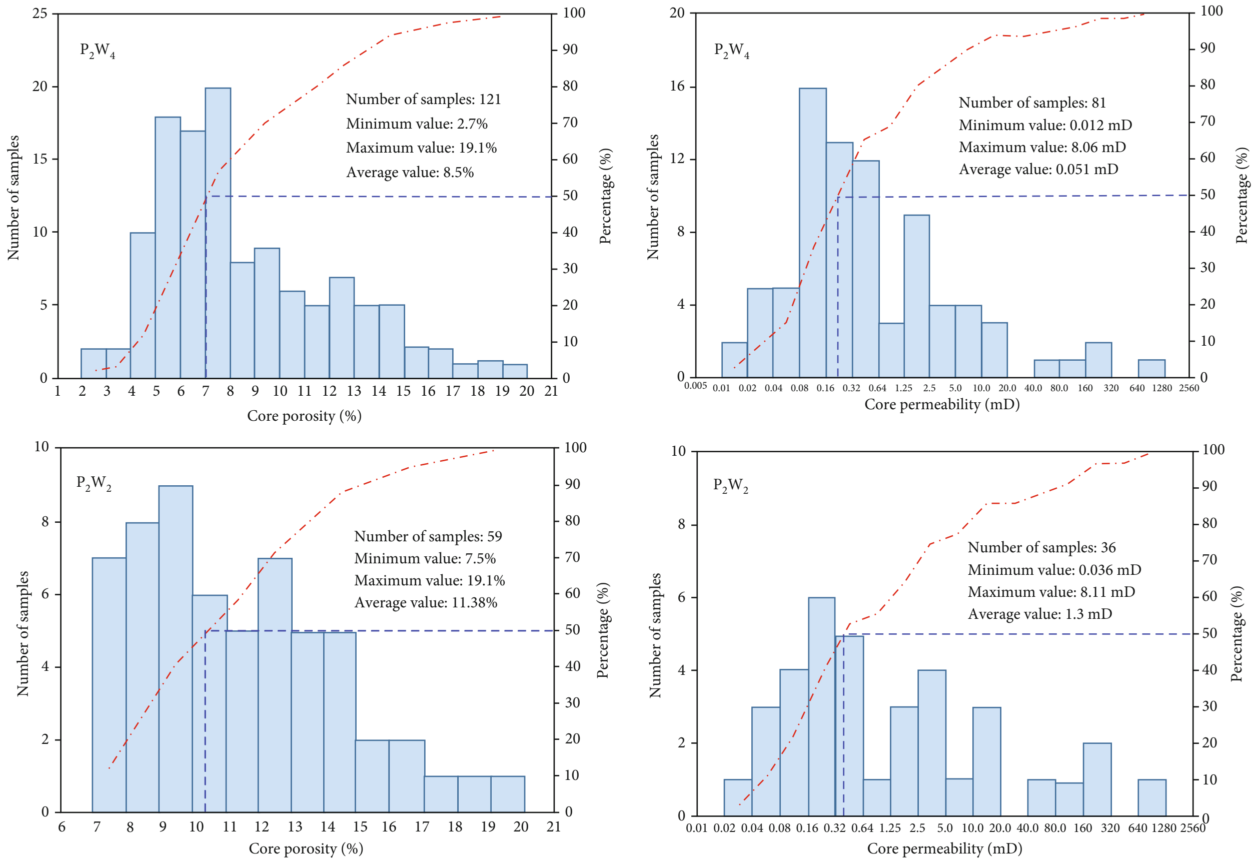

Figure 3: Parametric statistics of reservoir physical properties of the Lower Urho Formation in the YB4 area.

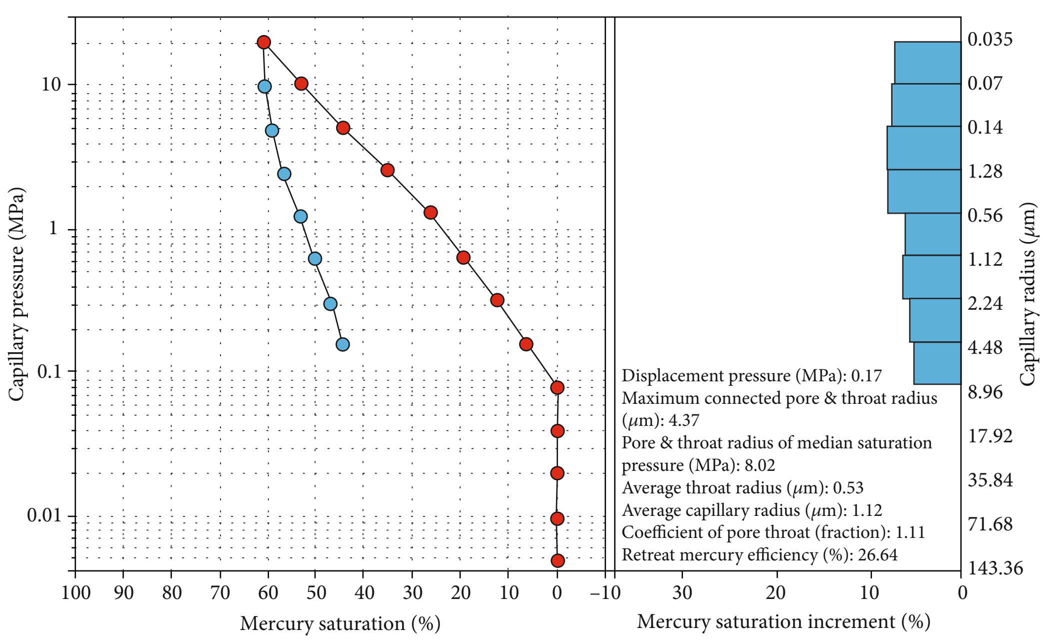

Figure 4: Typical capillary pressure curve of the Lower Urho Formation in the YB4 area (well YB4, 3915.3 m).

analcime ($NaAlSi_2O_7H_2$) and heulandite (($(Ca, Na_2)(Al_2Si_7O_{18})\cdot 6H_2O$)). By using the molecular formula of laumontite, the percentage content of Si, Al, and Ca was calculated as 23.78%, 11.73%, and 8.23%, respectively. Comparing laumontite with clay minerals, the Si/Al ratio of laumontite is not significantly different from that of clay minerals, whereas the Si/Ca ratio of laumontite is much lower than that of clay minerals (Table 2). Therefore, elemental logging can be used to differentiate laumontite from various clay minerals.

Table 2: Average content of chemical elements in turbidite and clay minerals.

Minerals	Si (%)	Al (%)	Ca (%)	Si/Al (%)	Si/Ca (%)
Laumontite	23.78	11.73	8.23	2.03	2.89
Kaolinite	21.24	20.52	0.38	1.04	55.89
Illite	23.92	12.26	0.42	1.95	56.95
Montmorillonite	22.88	8.35	1.13	2.74	20.25
Chlorite	12.42	10.92	0.48	1.14	25.88

5. Discussions

5.1. Logging Response Mechanism. Laumontite has an influence on the mineral composition, rock conductivity, and petrophysical properties of glutenite reservoirs. To ascertain the relationship between laumontite and the logging response in the reservoir, we conducted calibration using core analysis data to identify intervals containing laumontite within the study area. Furthermore, correlation analysis was performed among parameters such as reservoir logging lithology, mineral composition, petrophysical properties, and various logging curves.

5.1.1. Compensated Density Logging Response. The comparison of core skeletal density between samples containing laumontite and those without laumontite revealed that (Figure 5), in contrast to rock cores without laumontite minerals (with densities ranging from 2.554 to 2.655 g/cm^3), cores containing laumontite minerals exhibit significantly lower rock skeletal densities (ranging from 2.452 to 2.556 g/cm^3). This suggests the presence of minerals with lower skeletal densities within the rock composition. By referencing the mineral composition, content, and theoretical density logging values of different minerals in the corresponding well intervals, it is evident that the low-skeletal-density mineral in the reservoir is laumontite.

The base unit of laumontite's molecular structure is a tetrahedral arrangement formed by four oxygen atoms and one silicon (or aluminum) atom [38]. These silicon-oxygen (or aluminum-oxygen) tetrahedra then assemble to create unit rings, double rings, and cages (crystalline polyhedra), forming the three-dimensional framework structure of laumontite crystals. Various rings, acting as secondary units, combine to create the pores and channels in different types of laumontite. This unique crystal structure imparts laumontite with numerous uniformly distributed micropores, most of which have diameters below 1 nanometer. The abundance of micropores results in laumontite having a lower density compared to other framework silicate minerals of the same type, such as quartz and feldspar.

5.1.2. Compensated Neutron Logging Response. After performing corrections for mud content and porosity, an analysis was conducted to compare the neutron logging values between reservoirs containing laumontite and those without it (Figure 6(a)). The results indicated that in reservoirs without laumontite, neutron logging values primarily fall within the range of 6% to 10%, with an average of 8.8%. In contrast, the neutron logging values in reservoirs containing laumontite range from 11% to 19%, with an average of 14.6%. This indicates that glutenite reservoirs containing laumontite exhibit higher neutron logging values.

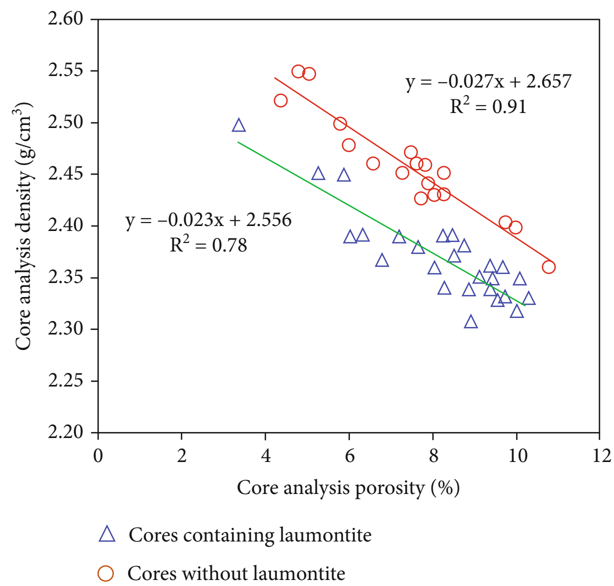

Figure 5: The comparison of core skeletal density between samples containing laumontite and those without laumontite.

Laumontite possesses a multitude of micropores, resulting in an extensive surface area, typically ranging between approximately 400 and 800 m^2/g. It can accommodate a significant amount of crystal water, contributing to the compensation of the hydrogen index measured by neutron logging. As a result, the neutron logging response values of laumontite-bearing glutenite reservoirs are significantly higher than that of rocks that do not contain laumontite.

5.1.3. Compensated Acoustic Logging Response. Similarly, after performing corrections on both mud content and porosity for the acoustic interval transit time logging values, an analysis was conducted to compare the acoustic interval transit time logging values between intervals containing laumontite and those without it. The results indicated that in reservoirs containing laumontite, the acoustic interval transit time values range from 52 μs/ft to 56 μs/ft, with an average value of 54.1 μs/ft. In contrast, in reservoirs without laumontite, the acoustic interval transit time values range from 52 μs/ft to 54 μs/ft, with an average value of 52.3 μs/ft (Figure 6(b)). This suggests that the acoustic interval transit

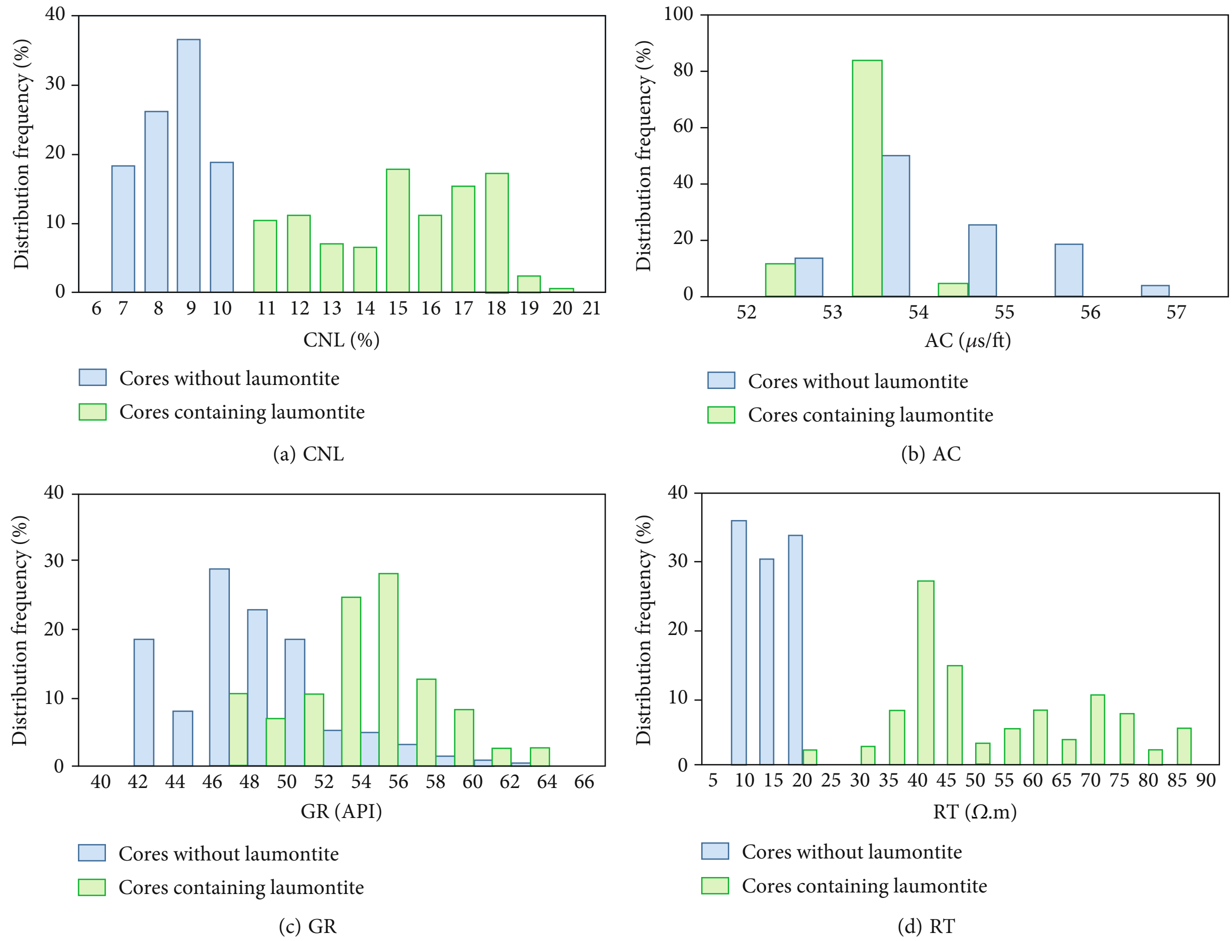

Figure 6: The statistics of CNL, AC, GR, and RT between samples containing laumontite and those without laumontite.

time values in laumontite-bearing reservoirs are similar to those in rocks composed primarily of quartz and feldspar.

With regard to the crystal structure type, laumontite is similar to minerals like quartz and feldspar, as they all belong to silicate minerals with a framework structure, whereas it differs significantly from layered silicate minerals like clay. According to the principle of the shortest propagation path for acoustic waves, since laumontite has an overall framework structure, acoustic waves propagate through the crystal skeleton rather than passing through crystal cavities. In contrast, the layered structure of clay minerals necessitates that acoustic waves pass through water molecules between the constituent clay layers, slowing down the propagation speed and increasing the propagation time. Additionally, the framework structure of laumontite contains numerous uniformly distributed micropores, most of which have diameters below 1 nanometer, with pore volume accounting for approximately 40%~50% of the total volume. Whether this micropore structure affects acoustic interval transit time has not been reported in relevant research to date, and the results of this experiment have not revealed any specific impact.

5.1.4. Gamma Ray Logging Response. In laumontite-bearing reservoirs, the natural gamma radiation values typically range from 44API to 52API, with the frequency peak corresponding to a GR value of 46API. In contrast, in reservoirs without laumontite, the resistivity values range from 48API to 60API, with the frequency peak corresponding to a GR value of 56API. The difference between the two is 10API, indicating that laumontite-bearing reservoirs exhibit a low GR characteristic (Figure 6(c)).

Natural laumontite is formed when mildly acidic volcanic glass material undergoes hydration, hydrolysis, reactions, and crystallization into rock in an alkaline water environment [39]. While the chemical composition of the volcanic glass material transforming into laumontite does not undergo significant changes in terms of components, there are noticeable changes in their concentrations. In laumontite rocks, the concentrations of SiO_2, Na_2O, and K_2O are significantly reduced compared to the original rock, while the CaO, MgO, Al_2O_3, and H_2O concentrations notably increase. In the study area, the laumontite minerals are primarily composed of non-K^+-bearing laumontite ($CaAl_2Si_2O_{12}4H_2{\bullet}O$), followed by analcime ($NaAlSi_2O_7H_2$) and heulandite ($(Ca, Na_2)(Al_2Si_7O_{18}){\cdot}6H_2O$). These minerals do not exhibit a high radioactivity. Under the effects of weathering and hydrolysis, the radioactive components in laumontite minerals are exchanged or lost and nonradioactive ions like Na^+ and Ca^{2+} precipitate. As radioactive minerals

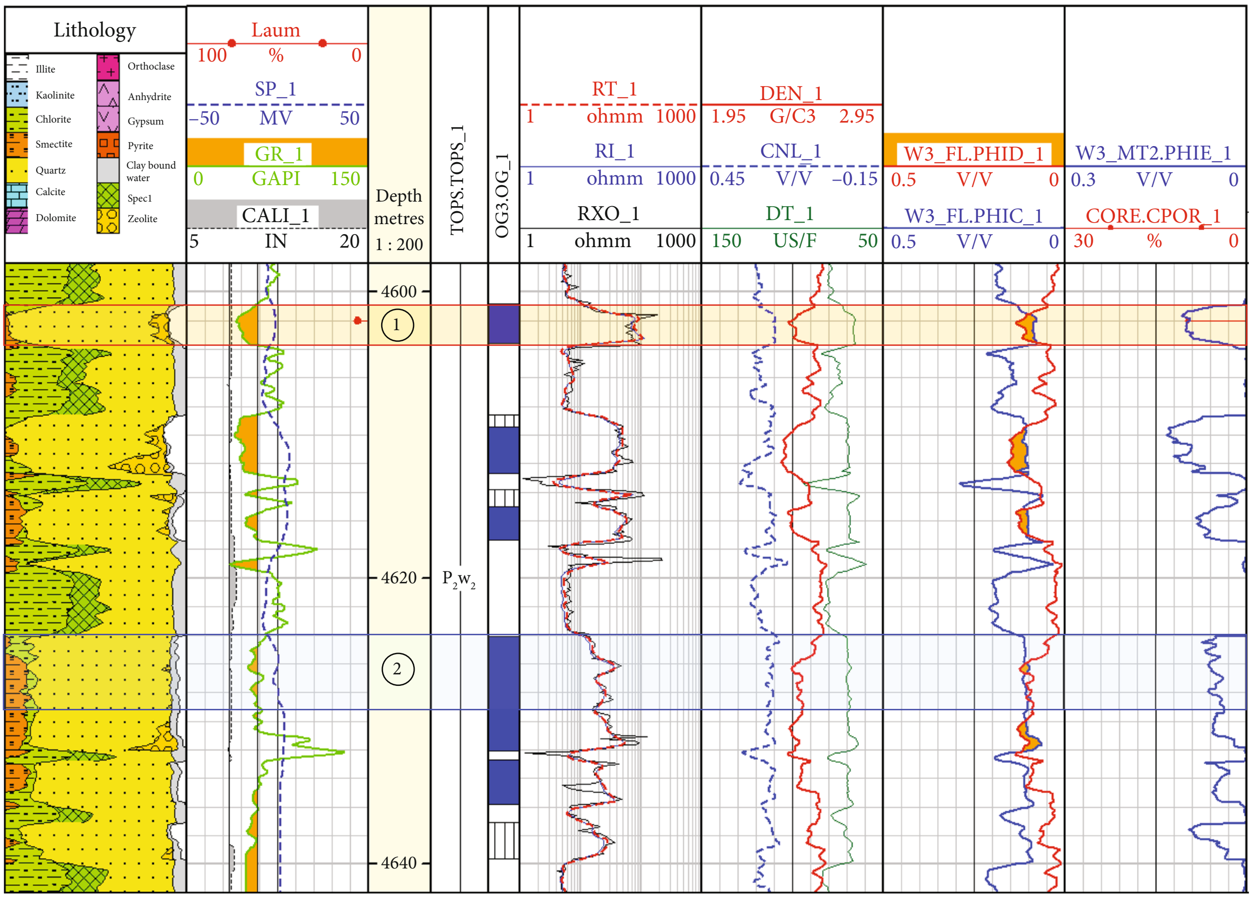

Figure 7: The comparison of resistivity between formation containing laumontite and those without laumontite (well YB2).

like K^+ decrease, the natural gamma radiation (GR) of the strata also decreases accordingly.

5.1.5. Resistivity Logging Response. The distribution of resistivity values of reservoir intervals containing laumontite and those without it indicated that in laumontite-bearing reservoirs, resistivity values range from 30 Ω·m to 90 Ω·m, with a mean of 47.8 Ω·m (Figure 6(d)). In contrast, in reservoirs without laumontite, resistivity values range from 5 Ω·m to 20 Ω·m, with an average of 12.5 Ω·m. The resistivity in laumontite-bearing reservoirs is significantly higher than that in strata without laumontite, demonstrating a high-resistivity characteristic.

In order to exclude the effect of oil content on high resistivity, the resistivity difference between zeolite-bearing and zeolite-free reservoir intervals with approximate petrophysical conditions and no hydrocarbon indications was analyzed. Taking YB2 well as an example (Figure 7), in the interval of 4600.5~4604 m, the rock sheet identification confirmed that the reservoir contains zeolite, with a resistivity value of 76 Ω·m. In the interval of 4624~4629.5 m, the reservoir does not contain zeolite, with a resistivity value of 19 Ω·m. These further indicate that the interval of zeolite-bearing reservoir is still with higher resistivity.

While the tetrahedral structure laumontite does have some cation exchange capacity, it differs from the equilib-

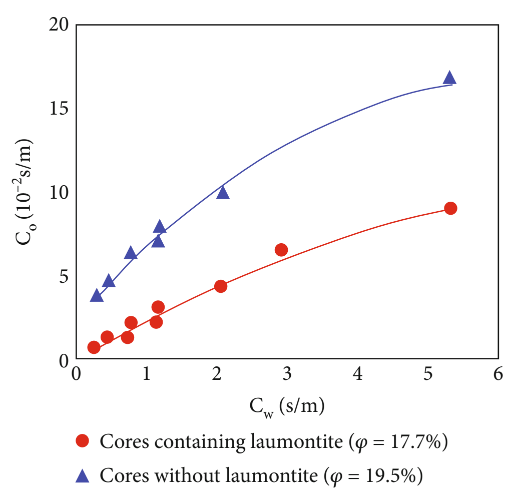

Figure 8: The comparison of Co-Cw relationship between samples containing laumontite and those without laumontite [40].

rium cations in the clay minerals with layered structures. The framework (caged) structure of laumontite limits the movement of equilibrium cations within its framework under the influence of electric fields, making it nonconductive or weakly conductive. Scholars have conducted rock electricity conductivity experimental analyses on the samples

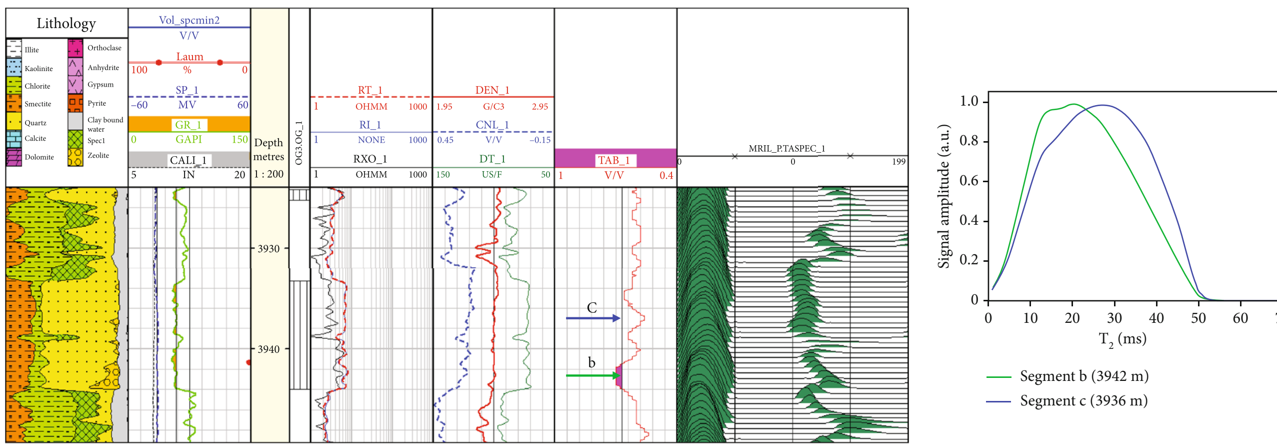

Figure 9: Distribution characteristics of NMR T_2 spectrum between samples containing laumontite and those without laumontite (well YB4).

containing laumontite and those without it in the Daqing Oil Field in China [40]. They found that rocks without laumontite had a higher electrical conductivity (Figure 8). The reason was due to that the laumontite's lattice contains a network of fine pores, slightly larger than nonhydrated cations; when laumontite is saturated with electrolyte solution, hydrated ions have difficulty migrating through this pore network, resulting in nonconductivity or weak conductivity of cations within laumontite. In contrast, laumontite crystals are formed in pore spacings due to diagenesis in later stages, which block the pores and lead to an increase in resistivity [41].

5.1.6. Nuclear Magnetic Resonance Logging Response. Comparing the distribution characteristics of the NMR T_2 spectrum between adjacent reservoir intervals containing laumontite (3942 m) and without laumontite (3936 m) in YB4 well (Figure 9), relative to the upper interval without laumontite (segment c), the T_2 spectrum peak in the laumontite-containing interval (segment b) appears farther to the left, and the distribution of signals in the short relaxation time part (<3 ms) is broader. The analysis suggests two reasons. On one hand, the presence of laumontite restricts the development of large pores due to its cementing effect. On the other hand, the laumontite's framework structure contains crystalline pores, accounting for approximately 40%~50% of the total volume, with a unique crystal structure that creates a significant number of uniform micropores (<1 nm). The relaxation signals in the NMR T_2 spectrum primarily originate from these micropore structures, while relaxation signals from larger pores are less prominent.

5.2. Quantitative Calculation of Laumontite Content. Experimental techniques such as XRD and electron probe analysis can provide mineral composition data with high precision. However, due to factors like testing costs and the discontinuity of core sampling along the borehole depth, it is challenging to obtain continuous mineral composition data along the well hole. Therefore, this paper uses a multimineral model optimization method to quantitatively calculate the laumontite content.

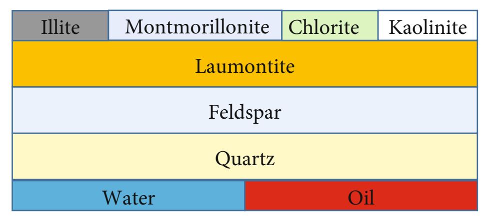

Figure 10: Multimineral model of laumontite-bearing glutenite reservoir.

The multimineral model optimization method is based on the principles of geophysical generalized inversion theory and component analysis [42, 43]. It assumes that geological formations with complex mineral components can be represented as combinations of locally homogeneous framework minerals, clay minerals, and pore fluids [44]. This method integrates well logging data and geological knowledge from specific regions into a multidimensional information complex. Then, optimization mathematical techniques can be used to find the best solution for this complex [45]. The interpretation process is as follows:

(1) Based on X-ray diffraction analysis, thin-section identification, and the characteristics of reservoir pore fluids, a multimineral model corresponding to the actual geological formation, which includes rock mineral components and pore fluids, was established

(2) Based on the multimineral model and the well logging response equations, a target function was established. Initial estimates for rock mineral components or pore fluid content were calculated. The target function and its gradient were computed, and convergence was checked. If convergence is not achieved, the estimated values are adjusted using the quasi-Newton method until convergence is reached

(3) Optimization quality checks and controls were carried out. If there is a significant difference between

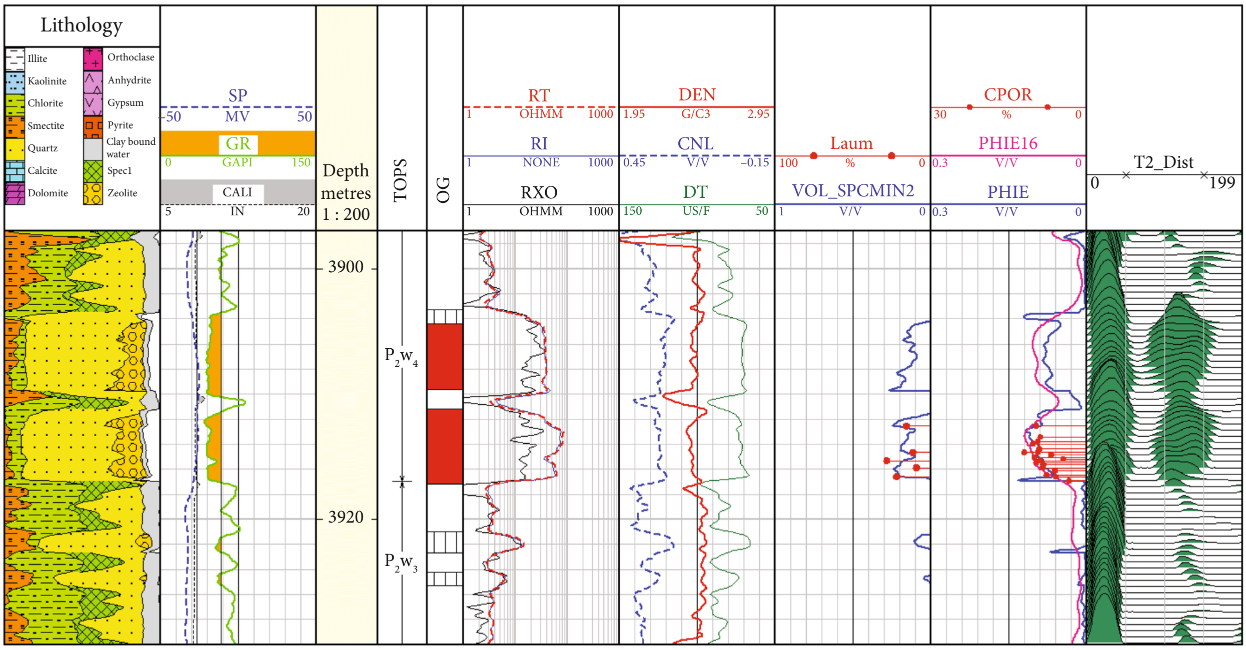

FIGURE 11: The calculation result of laumontite content based on multimineral model optimization method.

the theoretical computed logging curves and the actual logging curves, adjustments are made to the multimineral model, logging curve series, logging response values, and constraints. A new objective function is established, and this process is repeated until more than 68.5% of the values for each theoretical logging curve fall within the standard deviation range of the actual logging values. This process continues until the mineral composition or pore fluid content output aligns most closely with the actual geological conditions

5.2.1. Multimineral Model of Laumontite-Bearing Glutenite Reservoir. The multimineral model can be used to evaluate complex lithological reservoirs. Based on XRD analysis results and lithological characteristics of the glutenite reservoir in the study area, a multimineral component model was established (Figure 10). This model primarily covers the quartz, feldspar, clay minerals (illite, montmorillonite, chlorite, and kaolinite), and laumontite. The theoretical logging response parameters for each mineral were referenced from the Schlumberger Rock and Mineral Handbook.

5.2.2. Objective Function and Constraint Conditions. The theoretical logging response equation based on the multimineral model was established using sensitive logging curves such as neutron, density, gamma, resistivity, and sonic. The theoretical logging response values for geological formations can be described as follows according to the multimineral model.

$$f_i(A, x) = \sum_{j=1}^{k} a_{ij} \cdot \varphi_j, \tag{1}$$

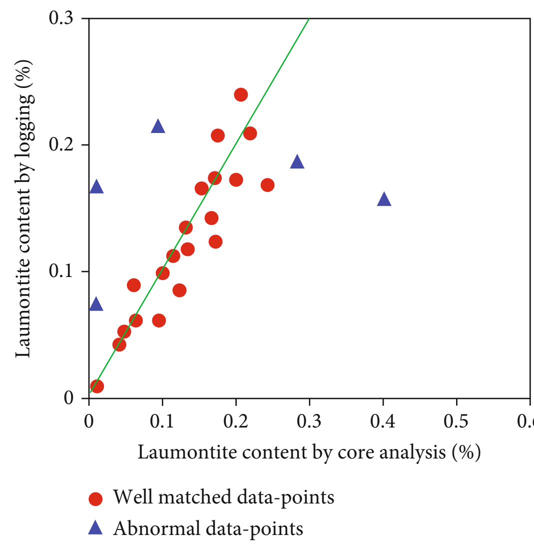

FIGURE 12: The comparison of laumontite content between multimineral model optimization method and core analysis.

where $f_i(A, x)$ is the theoretical logging response value for the ith logging curve, A is a matrix composed of a_{ij} elements, x is a vector composed of mineral composition or pore fluid content values to be solved, j is the total number of mineral compositions or pore fluids, k is the serial number of the mineral composition or pore fluid, a_{ij} is the theoretical logging response value of the ith logging curve for the jth mineral composition or pore fluid, and φ_j is the content of the jth mineral composition or pore fluid, expressed in percentage.

According to the principle of optimization, when the theoretical logging response values are closer to the actual logging values, the multimineral model can better reflect the actual geological conditions. A target function was established using nonlinear weighted least squares. In the case where the target function value is minimized, the smaller the difference between the theoretical logging response values and the actual logging response values, the more closely the mineral composition or pore fluid content obtained from the multimineral model to the actual geological conditions. The target function is defined as follows:

$$F(A, x)_{\min} = \sum_{i=1}^{m} \frac{d_i - f_i(A, x)^2}{\sigma_i^2 + \tau_i^2}, \tag{2}$$

where $F(A, x)_{\min}$ is the target function, i is the serial number of logging curve, m is the total number of logging curves, d_i is the actual logging response value for the ith logging curve, σ_i is the systematic error of the ith logging curve, and τ_i is the measurement error of the ith logging curve.

Because the sum of all components x_j in the column vector x is equal to 1, the following equation can be obtained:

$$\varphi + \sum_{j=1}^{p} \varphi_{clj} + \sum_{j=1}^{n} \varphi_{maj} = 1. \tag{3}$$

The content of each mineral component and pore fluid should conform to the geological characteristics. Range constraints on the content of each mineral component and porosity parameters need to be applied based on regional experience or actual test data, in order to make them more consistent with the actual distribution within a certain range.

5.2.3. Calculation Results of Laumontite Content. The optimization logging interpretation was carried out on the logging curves of 14 wells in terms of density, compensated neutron, natural gamma, and resistivity in the study area. The results indicated that, according to the confidence interval method, the theoretical logging curves closely match or are very close to the actual logging curves. On average, 87.5% of the theoretical values for all logging curves fall within the confidence intervals, which is significantly higher than the confidence probability of 68.3%. This suggests that the error between the theoretical and actual logging curve values is relatively small. The calculated contents of laumontite and effective porosity are in agreement with core analysis results, and their trends are consistent. The obtained curves of mineral component content show a good agreement with lithology (Figure 11).

Comparing the optimized results of the laumontite content calculated using the multimineral model optimization method with the core analysis data, it can be observed that more than 80% of the data points exhibit a good match (depicted as red solid circle dots). Data points that deviate to the left side above the diagonal line represent samples with a relatively low laumontite content, whereas data points located at the right side above the diagonal line indicate a laumontite content reaching around 30% to 50%, which are considered outliers (Figure 12).

6. Conclusions

In the study area, zeolite group minerals are primarily represented by laumontite, with analcime and heulandite as secondary components. These zeolite group minerals are present in the reservoir primarily as cement and fracture fillings. The zeolite-filled cementation suppresses the development of pore and throat structures, thereby negatively affecting the storage and permeability properties of the reservoir. As a result, reservoir intervals with zeolite-filled cementation exhibit a significantly lower porosity and permeability compared to those without zeolite-filled cementation.

Due to its water-bearing framework structure, laumontite contains numerous micropores and crystal water, which results in the logging characteristics of low natural gamma radiation values, low density, high neutron porosity, and high resistivity (two lows and two highs) in the conventional logging curves of laumontite-bearing formations. The acoustic interval transit time shows no significant differences, while the nuclear magnetic logging exhibits more pronounced short relaxations.

The optimization method constructed based on the multimineral model according to the target reservoir's lithological characteristics can effectively calculate the laumontite content. The match between the calculated laumontite content and the obtained laumontite content from core analysis exceeds 80%.

Data Availability

The original contributions presented in the study are included in the article; further inquiries can be directed to the corresponding author.

Conflicts of Interest

The authors declare that they have no known competing financial interests or personal relationships that could have appeared to influence the work reported in this paper.

Acknowledgments

This study was funded jointly by the Natural Science Foundation of Sichuan Province, P. R. China (Grant No. 2023NSFSC0260), and the Scientific Research Project of Mianyang Normal University (Grant No. QD2019A03).

References

[1] X. H. Yu, S. L. Li, C. P. Tan, J. H. Qu, C. Zhang, and C. F. Zhao, "Coarse-grained deposits and their reservoir characterizations: a look back to see forward and hot issue," *Journal of Palaeogeography*, vol. 20, no. 5, pp. 713–736, 2018.

[2] Z. Liu, D. F. He, and X. G. Tong, "Formation and distribution of giant oil and gas fields in North Sea Basin," *China Petroleum Exploration*, vol. 16, no. 3, pp. 31–43, 2011.

[3] C. C. Turner, B. T. Cronin, L. A. Riley, S. Patruno, and A. L. Jackson, "The South Viking Graben: overview of Upper Jurassic rift geometry, biostratigraphy, and extent of Brae Play submarine fan systems," *AAPG Memoir*, vol. 115, 2018.

[4] X. J. Pang, C. M. Niu, X. F. Du, Q. B. Wang, and L. M. Dai, "Quantitative characterization of differences in glutenite reservoir in the Member1 and 2 of Shahejie formation in the northeastern margin of Shijiutuo uplift, Bohai Sea," *Acta Petrolei Sinica*, vol. 41, no. 9, pp. 1073–1088, 2020.

[5] D. Z. Zhang, L. L. Chu, X. Li, and X. L. Wang, "Comprehensive sweet point evaluation and exploration results of tight glutenite reservoir in fault basin: a case study of the Lower Cretaceous Shahezi formation in Xujiaweizi fault depression in the northern Songliao basin," *China Petroleum Exploration*, vol. 27, no. 5, pp. 73–82, 2022.

[6] Y. C. He and C. R. Zhang, "The world's largest conglomerate oil field discovered in Junggar basin," *Xinjiang Geology in China*, vol. 44, no. 6, pp. 1174–1174, 2017.

[7] S. Y. Hu, X. J. Wang, Z. L. Cao, J. Z. Li, D. Y. Gao, and Y. Xu, "Formation conditions and exploration direction of large and medium gas reservoirs in the Junggar basin, NW China," *Petroleum Exploration and Development*, vol. 47, no. 2, pp. 266–279, 2020.

[8] D. W. Lei, G. Q. Chen, H. L. Liu, X. Li, K. Y. Abu, and J. C. Tao, "Study on the forming conditions and exploration fields of the Mahu giant oil (gas) province, Junggar basin," *Acta Geologica Sinica*, vol. 91, no. 7, pp. 1604–1619, 2017.

[9] Y. Tang, D. W. Lei, J. Cao, Y. Liu, L. L. Huang, and H. Li, "Total petroleum system and inner-source natural gas exploration in Permian strata of Junggar basin," *Xinjiang Petroleum Geology*, vol. 43, no. 6, pp. 654–662, 2022.

[10] K. L. Kra, L. Qiu, Y. Yang et al., "Sedimentological and diagenetic impacts on sublacustrine fan sandy conglomerates reservoir quality: an example of the Paleogene Shahejie formation (Es4s Member) in the Dongying depression, Bohai Bay basin (East China)," *Sedimentary Geology*, vol. 427, article 106047, 2022.

[11] J. P. Yan, J. Fan, M. Wang, Z. Z. Hu, H. Qin, and J. Chao, "Rock fabric and pore structure of the Shahejie sandy conglomerates from the Dongying depression in the Bohai Bay basin, East China," *Marine and Petroleum Geology*, vol. 97, pp. 624–638, 2018.

[12] W. Z. Yang, J. G. Hou, Y. M. Liu, L. X. Dou, and X. Wang, "The pore structures of different lithofacies in low-permeability sandy conglomerate reservoirs and their diagenetic impacts: a case study from the Es4member of the northern steep slope in Dongying depression, Bohai Bay basin, NE China," *Marine and Petroleum Geology*, vol. 136, no. 2, article 105481, 2022.

[13] M. Orhan, D. Henning, and H. Erik, "Diagenetic influence on reservoir quality evolution, examples from Triassic conglomerates/arenites in the Edvard Grieg field, Norwegian North Sea," *Marine and Petroleum Geology*, vol. 93, no. 5, pp. 247–271, 2018.

[14] R. L. Hay, *Zeolites and Zeolites Reacations in Sedimentary Rocks*, Geological Society of America, New York, 1966.

[15] A. Iijima, "A petrochemical aspect of the zeolite formation in volcaniclastic rocks," in *Proceedings of the 27th International Geological C: Utrecht*, pp. 29–52, VNU Science Press, 1984.

[16] J. R. Boles, *Zeolites in Low-Grade Metamorphic Rocks. Mineralogy and Geology of Natural Zeolites*, Mineralogical Society America, Washington D C, 1989.

[17] M. Utada, "Zeolitization in the continental margin, with special reference to those in the Green Tuff region in Japan," *Yerbilimleri*, vol. 13, no. 14, pp. 35–43, 1987.

[18] R. Surdam, "Secondary porosity formation in sandstone reservoir," *AAPG Bulletin*, vol. 68, pp. 485–493, 1984.

[19] S. S. Levy, *Petrology of samples from drill holes USW H-3, H-4, and H-5, Yucca Mountain, Nevada*, LOS Alamos NAT Lab-Rept, 1984.

[20] S. J. Chipera, F. Goff, C. J. Goff, and M. Fittipaldo, "Zeolitization of intracaldera sediments and rhyolitic rocks in the 1.25 Ma lake of Valles caldera, New Mexico, USA," *Journal of Volcanology and Geothermal Research*, vol. 178, no. 2, pp. 317–330, 2008.

[21] S. Zhu, X. Zhu, X. Wang, and Z. Liu, "Zeolite diagenesis and its control on petroleum reservoir quality of Permian in northwestern margin of Junggar basin, China," *Science China Earth Sciences*, vol. 41, no. 11, pp. 1602–1612, 2011.

[22] G. K. Moncure, "Zeolite diagenesis below Pahute Mesa, Nevada Test Site," *Clay & Clay Minrals*, vol. 29, no. 5, pp. 385–396, 1981.

[23] A. Iijima, "Zeolites in petroleum and natural gas reservoir," *Natural Zeolites Occurrence Properties Application*, vol. 45, no. 1, pp. 347–402, 2001.

[24] M. L. Fercia, R. Lonis, R. Peretti, S. Antonio, S. Antonello, and Z. Antonio, "Mineralogical characteristics and cationic exchange properties of a zeolite mineral from Romana, NW Sardinia, Italy," *Resource Geology*, vol. 59, no. 1, pp. 15–24, 2009.

[25] Z. Li, L. Qiu, Z. Shi, Y. Tang, Y. Kong, and S. Zhu, "Diagenesis of zeolite minerals and its significance for hydrocarbon accumulation in the second member of Jiamuhe formation of Zhongguai area, Junggar basin," *Journal of China University of Petroleum*, vol. 38, no. 1, pp. 1–7, 2014.

[26] S. Zhu, X. Zhu, D. Wu et al., "Alteration of volcanics and its controlling factors in the Lower Permian reservoirs at northwestern margin of Junggar basin," *Oil & Gas Geology*, vol. 35, no. 1, pp. 77–85, 2014.

[27] K. Xi, Y. Cao, H. Chang et al., "Diagenetic variations with respect to sediment composition and paleo-fluids evolution in conglomerate reservoirs: a case study of the Triassic Baikouquan formation in Mahu sag, Junggar basin, Northwestern China," *Journal of Petroleum Science & Engineering*, vol. 197, article 107943, 2021.

[28] Y. J. Wang, D. Jia, J. G. Pan et al., "Multiple phase tectonic superposition and reworking in the Junggar basin of Northwestern China—implications for deep-seated petroleum exploration," *AAPG Bulletin*, vol. 102, no. 8, pp. 1489–1521, 2018.

[29] Z. H. Kang, "Evolution of Paleozoic sedimentation of the Junggar basin," *Journal of Geomechanics*, vol. 8, no. 1, pp. 79–86, 2011.

[30] D. M. Moore and R. C. Reynolds, *X-Ray Diffraction and the Identification and Analysis of Clay Minerals*, Oxford University Press, Oxford, 1997.

[31] M. S. Rahner, M. Halisch, C. P. Fernandes, A. Weller, and S. Viviane, "Fractal dimensions of pore spaces in unconventional reservoir rocks using X-ray nano- and micro-computed tomography," *Journal of Natural Gas Science and Engineering*, vol. 55, no. 7, pp. 298–311, 2018.

[32] K. L. Xi, Y. C. Cao, Y. Z. Wang et al., "Factors influencing physical property evolution in sandstone mechanical compaction: the evidence from diagenetic simulation experiments," *Petroleum Science*, vol. 12, no. 3, pp. 391–405, 2015.

[33] Y. Li, Z. Zhang, H. Song, X. Zhou, J. Guo, and L. Zhu, "Evaluation of irreducible water saturation by electrical imaging

logging based on capillary pressure approximation theory," *Geoenergy Science and Engineering*, vol. 244, article 511592, 2023.

[34] E. D. Pittman, "Relationship of porosity and permeability to various parameters derived from mercury injection capillary pressure curves for sandstones," *AAPG Bulletin*, vol. 76, no. 2, pp. 191–198, 1992.

[35] M. Schmitt, C. P. Fernandes, J. C. Neto, F. G. Wolf, and S. Dos, "Characterization of pore systems in seal rocks using nitrogen gas adsorption combined with mercury injection capillary pressure techniques," *Marine & Petroleum Geology*, vol. 39, no. 1, pp. 138–149, 2013.

[36] L. S. Campbell, J. Charnock, A. Dyer et al., "Determination of zeolite-group mineral compositions by electron probe microanalysis," *Mineralogical Magazine*, vol. 80, no. 5, pp. 781–807, 2016.

[37] G. A. Ozin, A. Kuperman, and A. Stein, "Advanced zeolite materials science," *Angewandte Chemie*, vol. 101, no. 3, pp. 373–390, 1989.

[38] R. W. Grosse-Kunstleve, L. B. Mccusker, and C. J. Baerlocher, "Zeolite structure determination from powder diffraction data: applications of the FOCUS method," *Journal of Applied Crystallography*, vol. 32, no. 3, pp. 536–542, 1999.

[39] H. Y. Wu, Y. Tang, W. Sun, X. Y. Wang, and Q. S. Chang, "An analysis of the zeolite cement in sand-conglomerate and diagenetic mechanism of Jiamuhe formation, Zhongguai area, Junggar basin," *Acta Petrologica et Mineralogica*, vol. 37, no. 1, pp. 75–86, 2018.

[40] X. C. Qu, "Experimental study on the electrical properties of turbidite containing formations," in *Proceedings of the International Well Logging Academic Conference in 1994*, pp. 10–13, Petroleum Industry Press, Peking, 1994.

[41] L. Zhu, Y. Ma, J. Cai, C. Zhang, W. Shiguo, and X. Zhou, "Key factors of marine shale conductivity in southern China—Part II: the influence of pore system and the development direction of shale gas saturation models," *Journal of Petroleum Science and Engineering*, vol. 209, article 109516, 2022.

[42] M. Jiang, H. An, X. Gao, D. Liu, and X. Xie, "Consumption-based multi-objective optimization model for minimizing energy consumption: a case study of China," *Energy*, vol. 208, article 118384, 2020.

[43] W. Liu, C. Zhang, Z. Zhang et al., "A new method of mineral inversion based on error analysis and static response equation error: a case study of a shale gas reservoir in the Wufeng-Longmaxi formation," *Interpretation*, vol. 10, no. 1, pp. T117–T126, 2022.

[44] L. Zhu, J. Sun, X. Zhou et al., "Well logging evaluation of fine-grained hydrate-bearing sediment reservoirs: considering the effect of clay content," *Petroleum Science*, vol. 20, no. 2, pp. 879–892, 2023.

[45] L. Cheng, M. Prasad, R. J. Michelena et al., "Using rock-physics models to validate rock composition from multimineral log analysis," *Geophysics*, vol. 87, no. 2, pp. MR49–MR62, 2022.